2010

Glycine311, a determinant of paxilline block in BK channels: A novel bend in the BK S6 helix

Yu Zhou
Washington University School of Medicine in St. Louis
Qiong-Yao Tang
Washington University School of Medicine in St. Louis
Xiao-Ming Xia
Washington University School of Medicine in St. Louis
Christopher J. Lingle
Washington University School of Medicine in St. Louis

Published April 26, 2010

Glycine$_{311}$, a determinant of paxilline block in BK channels: a novel bend in the BK S6 helix

Yu Zhou, Qiong-Yao Tang, Xiao-Ming Xia, and Christopher J. Lingle

Department of Anesthesiology, Washington University School of Medicine, St. Louis, MO 63110

The tremorogenic fungal metabolite, paxilline, is widely used as a potent and relatively specific blocker of Ca^{2+}- and voltage-activated Slo1 (or BK) K^+ channels. The pH-regulated Slo3 K^+ channel, a Slo1 homologue, is resistant to blockade by paxilline. Taking advantage of the marked differences in paxilline sensitivity and the homology between subunits, we have examined the paxilline sensitivity of a set of chimeric Slo1/Slo3 subunits. Paxilline sensitivity is associated with elements of the S5–P loop–S6 module of the Slo1 channel. Replacement of the Slo1 S5 segment or the second half of the P loop results in modest changes in paxilline sensitivity. Replacing the Slo1 S6 segment with the Slo3 sequence abolishes paxilline sensitivity. An increase in paxilline affinity and changes in block kinetics also result from replacing the first part of the Slo1 P loop, the so-called turret, with Slo3 sequence. The Slo1 and Slo3 S6 segments differ at 10 residues. Slo1-G311S was found to markedly reduce paxilline block. In constructs with a Slo3 S6 segment, S300G restored paxilline block, but most effectively when paired with a Slo1 P loop. Other S6 residues differing between Slo1 and Slo3 had little influence on paxilline block. The involvement of Slo1 G311 in paxilline sensitivity suggests that paxilline may occupy a position within the central cavity or access its blocking position through the central cavity. To explain the differences in paxilline sensitivity between Slo1 and Slo3, we propose that the G311/S300 position in Slo1 and Slo3 underlies a structural difference between subunits in the bend of S6, which influences the occupancy by paxilline.

INTRODUCTION

Fungal metabolites include a variety of indole alkaloids, among which are the most potent nonpeptidergic blockers of Ca^{2+}- and voltage-activated Slo1 (KCNMA1) large-conductance Ca^{2+}-activated K^+ (BK)-type K^+ channels yet identified. Such compounds, including paxilline, penitrem A (Cole and Cox, 1981; Knaus et al., 1994), and lolitrem B (Imlach et al., 2009) block Slo1 channels at nM concentrations. Although scorpion toxins such as iberiotoxin and charybdotoxin (CTX) can also inhibit Slo1 channels at nM concentrations (Giangiacomo et al., 1992, 1993), Slo1 channels containing particular auxiliary β subunits exhibit resistance to block by such toxins (Xia et al., 1999; Meera et al., 2000; Xia et al., 2000). This renders the scorpion toxins less useful as tools for evaluating the role of Slo1 channels in native tissues. As a consequence, paxilline is increasingly used as a relatively potent and apparently relatively specific Slo1 channel blocker (Shao et al., 1999; Raffaelli et al., 2004; Tammaro et al., 2004; Essin et al., 2009). The mechanism and site of action of paxilline and other related compounds remain poorly understood. Block by paxilline has been proposed to involve an allosteric effect on Slo1 channel function (Sanchez and McManus, 1996). Various fungal indole alkaloids are also able to allosterically regulate binding of CTX to Slo1 channels (Knaus et al., 1994). Interestingly, some compounds increase CTX binding and others inhibit it, although all share the ability to block BK channels. The allosteric effect of paxilline on CTX binding argues that paxilline does not bind to the CTX binding site, which is known to involve the extracellular turret of the Slo1 channel (Giangiacomo et al., 2008), but indirectly alters the CTX binding affinity.

Here, we have explored the structural elements of Slo1 channels that may be required for inhibition by paxilline. We find that the pH-regulated Slo3 K^+ channel, a homologue of Slo1, is resistant to blockade by paxilline, and through a set of Slo1/Slo3 chimeras identify Slo1 S6 as necessary for paxilline block. Mutational analysis reveals that a critical glycine residue (G311) in Slo1 is essential to maintain high affinity block by paxilline and can restore paxilline sensitivity in constructs containing a Slo3 S6 segment. We hypothesize that the presence or absence of G311 defines two distinct conformations of the S6 helix, either allowing or negating block by paxilline.

Y. Zhou and Q.-Y. Tang contributed equally to this paper.
Correspondence to Christopher J. Lingle: clingle@morpheus.wustl.edu

Abbreviations used in this paper: BK, large-conductance Ca^{2+}-activated K^+; CTX, charybdotoxin; Po, open probability.

The Rockefeller University Press $30.00
J. Gen. Physiol. Vol. 135 No. 5 481–494
www.jgp.org/cgi/doi/10.1085/jgp.201010403

Published April 26, 2010

MATERIALS AND METHODS

General methods

Oocyte preparation, handling of RNA, and electrophysiological methods used here were identical to those described in other recent papers from this laboratory (Tang et al., 2009, 2010). All experiments used excised inside-out patches in which solution exchange at the pipette tip was accomplished with an SF-77B fast perfusion stepper system (Warner Instruments). Pipettes were typically 1–2 MΩ and were coated with Sylgard (Sylgard 184; Corning) before heat polishing. Gigaohm seals were formed while the oocytes were bathed in frog Ringer (in mM: 115 NaCl, 2.5 KCl, 1.8 $CaCl_2$, and 10 HEPES, pH 7.4). After patch excision, the pipette tip was moved into flowing test solutions. The pipette solution (bathing the extracellular membrane face) contained (in mM): 140 K-methanesulfonate, 20 KOH, 10 HEPES, and 2 $MgCl_2$, pH 7.0. The composition of the solution used to bathe the cytoplasmic face of the patch membrane was (in mM): 140 K-methanesulfonate, 20 KOH, and 10 HEPES, with pH adjusted to 7.0. For 0 Ca^{2+}, the solution also contained 5 mM EGTA. For 10 µM Ca^{2+}, it contained 5 mM HEDTA, and for 100 or 300 µM Ca^{2+}, no Ca^{2+} buffer was included. For 10 µM Ca^{2+}, the solution was titrated with a Ca methanesulfonate solution to obtain the desired Ca^{2+} concentration (Zhang et al., 2001), as defined with a Ca^{2+}-sensitive electrode calibrated with commercial Ca^{2+} solutions (WPI). Measurements and fitting of current recordings was accomplished either with Clampfit (MDS Analytical Technologies) or with programs written in this laboratory. Experiments were performed at room temperature (~22–25°C).

Steady-state current measurements were used to calculate conductances with the assumption of a 0-mV reversal potential. Conductances at each voltage and drug concentration for any given patch were normalized to the maximum conductance (G/G_{max}) measured under any condition for that patch. Conductance–voltage (G-V) curves were then generated from the mean estimates for the set of patches. When the time course of blocker onset was examined, depolarizing test pulses of 3–20 ms were applied at frequencies of 0.2/s to 1/s among different patches. For constructs in which stronger depolarizations were required for more robust current activation, slower frequencies were used to minimize the possibility of patch destruction. The brief duration of the test steps (3–20 ms) produced no time-dependent changes in block (or unblock), so variation in stimulus frequencies will not impact on the extent of block observed in these experiments. For example, variations in stimulus frequency between 1 and 0.2 Hz did not alter the time course or extent of block by paxilline of Slo1.

Constructs

The coding region of mSlo1 (GenBank accession no. NM_010610; provided by L. Salkoff, Washington University School of Medicine, St. Louis, MO) was subcloned into the pXMX oocyte expression vector (Tang et al., 2009). The mSlo3 construct (Schreiber et al., 1998) was also obtained from L. Salkoff with updated information regarding Slo3 given in GenBank accession number AF039213 (Zhang et al., 2006a). The DN5 chimeric construct (also termed 1P3C), in which the Slo1 cytosolic domain is replaced with the Slo3 cytosolic domain, has been described previously (Xia et al., 2004). Slo1/Slo3 chimeric constructs were generated by standard overlapping PCR methods used in the laboratory and were composed of the following: MC13: $Slo1_{1\text{-}182}$:$Slo3_{171\text{-}end}$; MC2: $Slo1_{1\text{-}233}$:$Slo3_{223\text{-}314}$:$Slo1_{326\text{-}end}$; MC6: $Slo1_{1\text{-}258}$:$Slo3_{248\text{-}288}$:$Slo1_{300\text{-}end}$; MC8: $Slo1_{1\text{-}258}$:$Slo3_{248\text{-}268}$:$Slo1_{280\text{-}end}$; MC10: $Slo1_{1\text{-}299}$:$Slo3_{289\text{-}314}$:$Slo1_{326\text{-}end}$; MC18: $Slo1_{1\text{-}279}$:$Slo3_{269\text{-}288}$:$Slo1_{300\text{-}end}$.

The sequences of the segments evaluated in the S5–P loop–S6 segment are:

S5:
```
Slo1 235 LVNLLSIFISTWLTAAGFIHLVEN 258
Slo3 224 LSKLLSIVISTWFTAAGFLHLVEN 247
```

First half P loop (turret residues):
```
Slo1 259 SGDPWENFQNNQALTYWECVY 279
Slo3 248 SGDPWLNGRNSQTMSYFESIY 268
```

Second half of P loop (pore helix and selectivity filter):
```
Slo1 280 LLMVTMSTVGYGDVYAKTTL 299
Slo3 269 LVTATMSTVGFGDVVAKTSL 288
```

S6:
```
Slo1 300 GRLFMVFFILGGLAMFASYVPEIIELI 326
Slo3 289 GRIFIVFFTLGSLILFANTIPEMVELF 315
```

Many of the chimeras used in this study exhibit interesting gating behaviors, including shifts in activation gating, gating kinetics, and persistent current activation at negative voltages. Future study of such chimeras may prove useful in regards to investigation of allosteric regulation of this family of channels. However, here we are simply concerned with whether aspects of block by paxilline are retained or abolished.

Estimates of block affinity

The specific molecular mechanism of block by paxilline is not known. Here, to provide an estimate of relative paxilline sensitivity of different constructs, we assume that paxilline blocks both open and closed states, and that block of G-V curves is defined by block occurring at the holding potential. This assumption is based on the fact that both the rates of paxilline block onset and recovery are slow relative to the duration of the voltage steps used to define block. Furthermore, there is no indication of any time-dependent block or unblock during the voltage steps used to define BK conductance. Thus, block observed at any test potential is likely to be that observed during the holding potential conditions. To describe activation, we used the allosteric model of BK channel activation (Horrigan and Aldrich, 2002) in which open probability (Po) is defined by three independent conformational equilibria: L (voltage dependence z_L), J (voltage dependence z_J), and K, reflecting the channel closed–open equilibrium, the voltage sensor equilibrium, and the Ca^{2+} binding constant, respectively. D, C, and E correspond to constants for coupling between voltage sensor movement to channel activation (D), between Ca^{2+} binding and channel activation (C), and between Ca^{2+} binding and voltage sensor activation (E). Defining

$$1/\bar{L} = \frac{1}{L}\left(\frac{1+J+K+JKE}{1+JD+KC+JDKCE}\right)^4,$$

channel Po as a function of voltage, Ca^{2+} and paxilline concentration for a model that involves block of both open and closed states is given in Eq. 1:

$$Po(Ca,V,[pax]) = \frac{1}{1+\frac{1}{\bar{L}}+\frac{1}{\bar{L}}\frac{[pax]}{K_{bc}}+\frac{[pax]}{K_{bo}}}, \quad (1)$$

where K_{bc} and K_{bo} are blocking affinities of paxilline for closed and open channels, respectively.

Given that there appears to be no equilibration of the blocking equilibrium during test steps, the applicability of Eq. 1 also requires that, at the holding potential, $K_{bc} = K_{bo}$, because otherwise Eq. 1 would predict some reequilibration in the steady-state G-V curves. In such a case, we define $K_b = K_{bc} = K_{bo}$.

Is it appropriate to use Eq. 1 for the set of constructs examined here, when the allosteric constants for each construct have not

Published April 26, 2010

been defined? Because we only examine paxilline block for a single activation condition, the specific terms for activation are not critical in defining blocking constants, as long as the assumption regarding saturating Po is reasonably valid. Here, for all constructs in which the pore domain largely arises from Slo1, we have constrained the fits such that the limiting Po at maximal activation is close to 1.0. In contrast, for MC13-S310G, we have assumed a Po at +300 mV of 0.35, appropriate for MC13 and Slo3 (Zhang et al., 2006b; Tang et al., 2010). In this case, the G-V curve was renormalized to a maximum value of 0.35 at +300 mV before application of Eq. 1.

Because we are not concerned about the detailed mechanism of paxilline here, we simply use Eq. 1 as an empirical description of paxilline effectiveness. It should be noted that if, at the holding potential, most channels (for all constructs examined here) are in closed states and there is little block or unblock during test steps, the value of K_{bo} would not be well-defined by the G-V curves. As such, the estimates obtained from Eq. 1 most likely reflect primarily estimates of closed-channel block under the holding conditions. For all experiments shown in this paper, patches were held at 0 mV at the indicated ligand concentrations, with a brief 10-ms step to −140 mV before steps to more depolarized test potentials.

One other aspect of paxilline block should be mentioned. It has been previously reported that paxilline block is associated with a rightward shift in G-V curves, particularly at low paxilline concentrations (Sanchez and McManus, 1996). Such a behavior is inconsistent with Eq. 1 and is also seen in Fig. 1 C as paxilline is increased from 0 to 5 nM (but not with additional paxilline increases). However, in tests using a single 100-nM paxilline concentration with full recovery after washout of paxilline, we have not seen this phenomenon. We therefore suspect it may arise from shifts in G-V curves unrelated to paxilline that can arise in some patches during long duration recordings. However, to assess how such a shift might impact on our estimates of block affinity, we also fit the G-V curves in two other ways. First, with the assumption that the G-V shift is part of the action of paxilline and reflects a stronger affinity of paxilline for closed channels (but no intrinsic voltage dependence of binding to either state), fitting with Eq. 1 yielded a closed-channel block affinity that was 3.1 ± 0.3 nM, whereas the open-channel block affinity was 13.8 ± 0.53 nM. In this case, Eq. 1 would only strictly be applicable if the currents reflect a steady-state condition (which we have already argued is most certainly not the case). In fact, to account for the weaker block with depolarization seen in the G-V curves, one would expect to see a time-dependent unblock; this is not seen in the current traces, therefore arguing against a gating shift as being part of paxilline action. Second, assuming that the G-V curve shift reflects a 16-mV shift during the initial 15–30 min of recording, a fit of a state-independent model to the G-V curves obtained solely in the presence of paxilline yielded a block affinity of 12.0 ± 0.7 nM. These considerations indicate that, regardless of the assumptions regarding blocking model, the blocking affinity of paxilline on Slo1 is ∼10–15 nM when patches are held at 0 mV with 10 µM of cytosolic Ca^{2+}. Thus, for comparative purposes, regardless of how one treats those datasets that may exhibit shift, Eq. 1 with the assumption that $K_{bo} = K_{bc}$ provides a useful measure of apparent block affinity.

The details of the fitting procedure are as follows. First, in fits of control G-V curves in the absence of blocker, z_L, z_J, and E were constrained to 0.3 *e*, 0.58 *e*, and 2.4, respectively, whereas C was generally constrained to 8 and D to 11 (Horrigan and Aldrich, 2002). The best-fit values for L and J were then determined; however, based on confidence limits, these values are not strongly constrained by the data when only a single Ca^{2+} concentration is used. To fit the G-V curves in the presence of blocker, terms for channel activation were then constrained to the best-fit values to the activation G-V alone, whereas parameters for blocking models were then defined through the best fit to the full set of G-V curves in the presence of paxilline. The fitting of functions to various datasets was done with a Levenberg-Marquardt nonlinear least-squares fitting algorithm implemented within software developed within this laboratory.

From the application of Eq. 1, we obtain an estimate for block affinity along with the 90% confidence limits returned by the fitting algorithm. For two constructs for which there is no overlap in the 90% confidence limit, there is a <10% likelihood that the observed difference would occur by chance. For the constructs examined here, pairwise comparisons suggest statistically significant differences among most pairs we have examined, even when the estimated blocking affinities differ by less than twofold. Because of concern about the reliability of blocker affinity estimates, in addition to the estimates in Fig. 1 (K_b = 10.6 ± 0.5 nM), we have also examined paxilline block of Slo1 for three other sets of patches: one set used to test whether paxilline produces gating shifts, another in which the experiments were all done in the presence of DTT, and another in which we tested the Ca^{2+} dependence of paxilline block. For these three cases, the paxilline estimates for apparent block affinity were 22.0 ± 0.4 nM (100 nM paxilline alone; n = 4 patches), 13.6 ± 0.7 (50 nM paxilline alone; n = 7), and 5.6 ± 0.2 (10 and 100 nM paxilline; n = 5). In other cases, we have noted apparently weaker block by paxilline. Thus, estimates of blocking affinity among different datasets may vary appreciably, even though the confidence limits associated with any individual estimate are small. Such differences are likely influenced by the challenges of working with a sticky blocking drug. For example, for experiments done over different periods of time, there may be differences in nominal drug concentration resulting from slight differences in drug preparation and delivery (see below). The binding of paxilline to various surfaces during preparation and delivery or differences in the average time between drug preparation and delivery to the set of patches might impact on the final effective concentrations. Because of the demonstrated variation in affinity estimates among sets of Slo1 patches, the focus of the present experiments is therefore primarily on large differences in paxilline affinity.

Molecular modeling

The structure of the BK channel S5–pore loop–S6 domain (Fig. 2 A) was generated based on homology modeling using Modeller 9v4 (Sali and Blundell, 1993). The Kv 1.2 structure (Long et al., 2005) was used as a template because there are no residue gaps between the BK channels and Kv 1.2. The cartoon in Fig. 2 A was generated using UCSF Chimera (Pettersen et al., 2004). The paxilline space-filling model was generated and optimized using Chem3D Pro (version 3.5.1; CambridgeSoft).

Chemicals

Salts for solution preparation were obtained from Sigma-Aldrich. Paxilline was obtained from Sigma-Aldrich. A 10-mM paxilline stock solution was prepared in 100% DMSO, and a 0.5-mM stock solution of paxilline was in 50% DMSO and stored at −20°C. Paxilline solutions used for experiments were prepared the day of an experiment and only used up to ∼4 h. To minimize loss of paxilline by binding to plastic surfaces, preparation of solutions was done entirely with glass beakers and pipettes. Paxilline solutions were delivered to patches via a multi-barrel pipette, with a glass perfusion line with Teflon junctions connecting the glass syringe reservoir to the delivery pipette. Even with glass components, there appeared to be some loss of paxilline in the reservoir over several hours, presumably due to binding to surfaces. DMSO was present in the final solutions at 0.05% for 500 nM paxilline, the highest concentrations tested. The paxilline concentrations found to be effective in our hands are several-fold higher than those reported in the initial studies on paxilline action (Knaus et al.,

Published April 26, 2010

1994; Sanchez and McManus, 1996). However, the concentrations we have found effective are similar to results in other recent work (Imlach et al., 2008). Aflatrem was from a 3-mg sample provided by D. Covey (Washington University School of Medicine, St. Louis, MO) in 1996, and the nominal concentrations reported here assume no degradation during that period. Aflatrem was made up as a 500-μM stock in 50% DMSO and used at nominally 10 nM (0.001% DMSO). Penitrem A and verruculogen were obtained from Alomone Laboratories, prepared as 1-mM stocks in 50% DMSO and used at 10 nM with 0.0005% DMSO.

RESULTS

Properties of block of macroscopic Slo1 currents by paxilline

The blockade of Slo1 channels by paxilline was studied in inside-out patches by examination of fractional block with different concentrations of paxilline at different activation voltages. The blocking effect of different paxilline concentrations at +120 mV on Slo1 currents activated with 10 μM Ca^{2+} is shown in Fig. 1 A. The concentration dependence of paxilline block was determined by sequential application of increasing concentrations of paxilline, with the duration of application of each concentration being sufficient to reach an apparent steady-state level of block (Fig. 1 B). After the application of 100 nM paxilline, patches were washed in control saline to ensure that currents recovered to near control levels, although full recovery was difficult to achieve. The inhibitory effects of paxilline were determined by measurement of steady-state current levels at different activation voltages (Fig. 1 C). Qualitatively, in some sets of patches we have observed that paxilline produces a greater fractional block at more negative activation voltages (Fig. 1 C), consistent with a positive shift in the G-V curves in the presence of paxilline, as reported by Sanchez and McManus (1996). Similar to their results, we also observed that any apparent G-V shift saturated at paxilline concentrations well below those producing maximal block of outward current. This discrepancy between the gating shifts and the fractional block of BK current suggests that they may arise from unrelated mechanisms. Because Slo1 G-V curves generated from

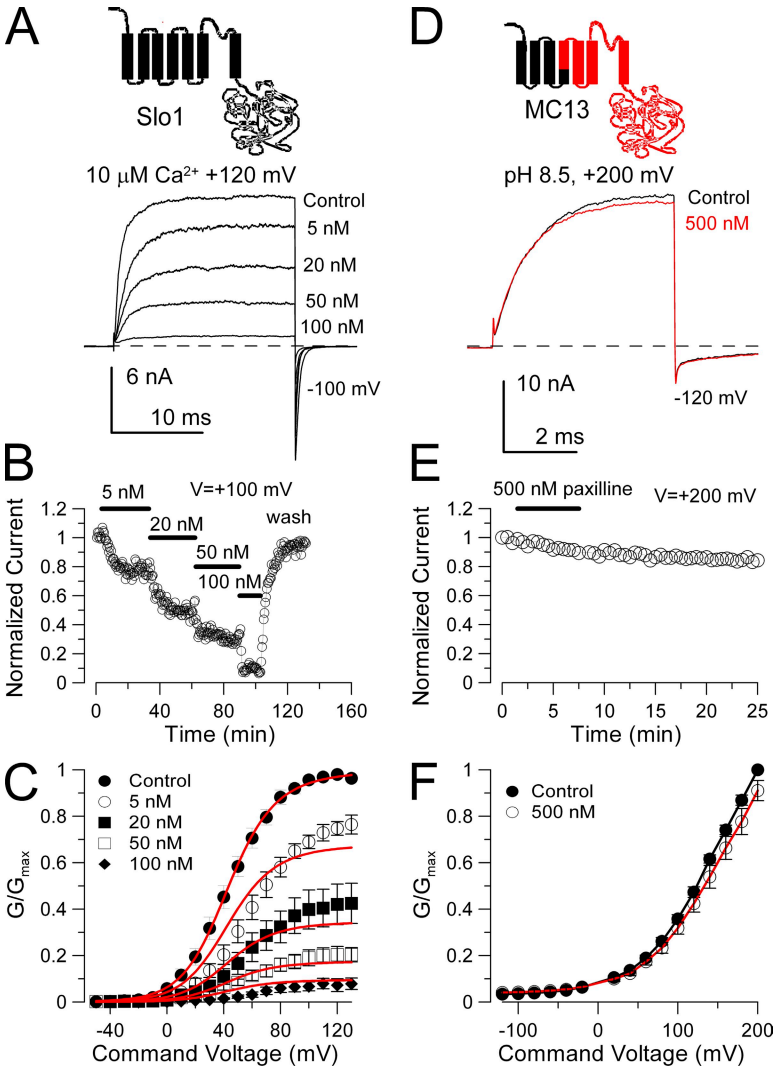

Figure 1. Paxilline blocks Slo1, but not Slo3 current. (A) Traces show block of Slo1 by paxilline, and the general topology of the Slo1 α subunit is shown on the top. Currents were activated by a step to +120 mV in an inside-out patch exposed to 10 μM Ca^{2+} with the indicated concentrations of paxilline. The holding potential was 0 mV, but the command steps were preceded by a brief 10-ms step to −140 mV. (B) The time course of paxilline block and unblock of Slo1 current is illustrated. Steps were to +100 mV. (C) G-V curves were generated from steady-state current levels for recordings in the absence and presence of paxilline (n = 4–7 patches). For this set of data, paxilline was applied at increasing concentrations, and full washout was not usually achieved (see B). Red lines correspond to a fit of Eq. 1, with K_b = 10.6 ± 0.49 nM with $z_c = z_o = 0$ *e*. (D) 500 nM paxilline is without effect on MC13 currents activated at +200 mV with pH 8.5. The composition of the MC13 construct is schematized at the top with Slo3 sequence shown in red. (E) MC13 currents are unaltered by 500 nM paxilline during 6 min of application. (F) 500 nM paxilline has little effect on MC13 G-V curves.

Published April 26, 2010

currents recorded in inside-out patches may show some positive shifts during the first 10 or 20 min of recording, we were concerned about the origins of the apparent G-V shift during the long times required to collect data in paxilline. In a separate set of four patches, we limited paxilline application to a single concentration of 100 nM. In this case, we observed an ~8-mV average positive shift in the presence of paxilline, but this shift did not reverse with paxilline washout. We are therefore unable to conclude that paxilline is responsible for small positive shifts in the Slo1 G-V curves.

To provide an estimate of the blocking effectiveness of paxilline on Slo1 current, we fit the family of G-V curves to Eq. 1, assuming identical block of both open and closed channels, as described in Materials and methods. This provides an apparent block affinity estimate that can be used for comparison to other constructs. From Eq. 1, this yielded an estimate of paxilline block affinity of 10.6 ± 0.5 nM.

The pH-regulated Slo3 channel is resistant to blockade by paxilline

The pH-regulated Slo3 channel does not express robustly in *Xenopus* oocytes (Zhang et al., 2006a). To allow investigation of many aspects of Slo3 function without challenges of poor expression, we have created a Slo1/Slo3 chimeric construct, termed MC13, which retains the characteristic functional properties of Slo3, including pH and voltage dependence, single-channel properties, and gating behavior (Tang et al., 2010). This construct replaces S0, S1, S2, and part of S3 of Slo3 with homologous sequence from Slo1 (see Materials and methods). Replacement of S0 alone was insufficient to enhance Slo3 expression. MC13 currents were activated in inside-out patches with pH 8.5 and positive voltage steps (Fig. 1 D). MC13 currents were essentially insensitive to 500 nM paxilline (Fig. 1, E and F). In other experiments, 100 nM paxilline was without effect when applied for over 30 min. The lack of effect of 500 nM paxilline on MC13 indicates that Slo1 is at least three orders of magnitude more sensitive to paxilline.

Paxilline sensitivity is determined by elements within the S5–pore loop–S6 segments of Slo1

To assess potential determinants of paxilline block, we focused our attention on the portion of the Slo1 and Slo3 channels that contain the S5–pore loop–S6 segments (Fig. 2 A). Chimeric constructs were created involving four segments within this region, S5, the first part of the pore loop, the second half of the pore loop, and then S6 (Table I and Fig. 2 A). Fig. 2 A also illustrates the relative size of a paxilline molecule compared with the Slo1 S5–S6 domain, whereas the chemical composition of paxilline is provided in Fig. 2 B.

When the entire S5–pore loop–S6 in Slo1 was replaced with the Slo3 sequence, currents from the resulting construct (MC2) were entirely resistant to block by 500 nM paxilline (Fig. 3, A and B). When the Slo1 S5 segment was replaced with the Slo3 sequence (MC28), blockade by 50 nM paxilline was retained (Fig. 3, C and D). A fit of Eq. 1 with the assumption of state independence and no voltage dependence yielded a blocking constant of 30.4 ± 1.7 nM. In contrast, when the Slo1 S6 segment was replaced by the Slo3 sequence (MC10), 100 nM paxilline had no effect (Fig. 3, E and F). This set of chimeras establishes that some feature of Slo1 S6, either specific residues or structure, is essential for blockade by paxilline.

The Slo1 pore helix also influences effectiveness of block by paxilline

Chimeras were also examined in which parts of the Slo1 pore loop were replaced with the Slo3 sequence.

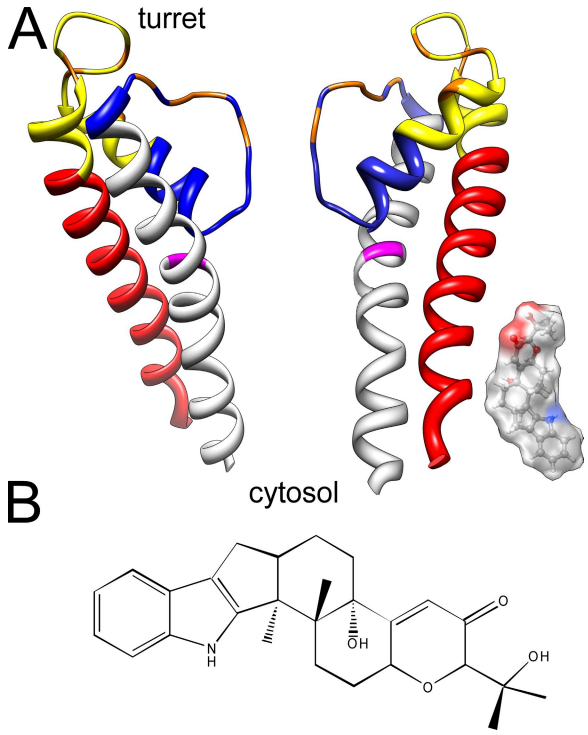

Figure 2. S5–pore loop–S6 segments of the BK channel and the relative size of the paxilline molecule. (A) A homology model of the BK channel S5–pore loop–S6 structure was generated based on alignment with Kv1.2 and the available Kv1.2 crystal structure. Coloring identifies segments used for generation of chimeras as follows: red, S5; yellow, first half of pore loop; blue, second half of pore loop, including so-called turret; gray, S6. Orange residues are those that influence iberiotoxin binding (Giangiacomo et al., 2008). G311 in S6 is highlighted in magenta. A space-filling model of paxilline (to the same scale) is positioned adjacent to an S5 helix, but this positioning is not meant to imply anything about the position of paxilline in a blocking site. Note that the actual topology of the BK turret is entirely unknown. Furthermore, this cartoon does not take into account the likely large width of the BK central cavity. (B) The chemical structure of paxilline is shown.

Published April 26, 2010

In construct MC6, in which the entire Slo1 pore loop was replaced with the Slo3 sequence, paxilline sensitivity only slightly reduced (two- to threefold) compared with wild-type Slo1 (Fig. 4 A). The estimated blocking affinity of paxilline for MC6 assuming state-independent block was $K_b = 23.2 \pm 1.0$ nM. When only the second half of the Slo1 P loop (residues 280–299) was replaced with the Slo3 sequence (construct MC18), paxilline sensitivity was also reduced about threefold compared with Slo1 (for MC18, $K_b = 30.0 \pm 1.4$) (Fig. 4 B). In contrast, when only the first half of the P loop was replaced with the Slo3 sequence (MC8), the paxilline block affinity was increased about twofold ($K_b = 4.04 \pm 0.10$ nM) relative to Slo1 (Fig. 4 C). These results suggest that the composition of the pore helix may impact on the ability of paxilline to block BK channels, perhaps reflecting the ability of tremorogenic alkaloids including paxilline to influence CTX binding to smooth muscle BK channels (Knaus et al., 1994).

Because estimates of blocking affinity among different constructs might be expected to vary on the order of up to two- to threefold (see Materials and methods) for a slow-acting, sticky blocker like paxilline, we sought independent tests to see if altering the pore loop segment impacts on paxilline affinity. For MC8, the apparently stronger paxilline block affinity is correlated with pronounced effects on blocking rates. The rate of onset of paxilline block for MC8 was clearly faster than for Slo1, even when MC8 was blocked with a fivefold lower concentration (Fig. 5, A and B). The effective forward rate of block for MC8 was ~10-fold faster than for block of Slo1 ($P < 0.0005$; *t* test assuming equal variance) (Fig. 5 C). In contrast, recovery from paxilline block of MC8 was not statistically different from that for Slo1 (Fig. 5 B; $P > 0.2$). Assuming a simple first-order blocking reaction, with $\tau_{on} = 1/(k_{on} + k_{off})$ and $\tau_{off} = 1/k_{off}$, effective first-order blocking rates and blocking constants were calculated (Fig. 5 C). The forward rates of block were 0.13×10^6 $M^{-1}s^{-1}$ and 1.45×10^6 $M^{-1}s^{-1}$ for Slo1 and MC8, respectively. Blocking constants estimated from the rates were 48.8 ± 5.9 nM and 6.8 ± 1.6 nM for Slo1 and MC8, respectively. In contrast, if the steady-state conductances for these same sets of patches were

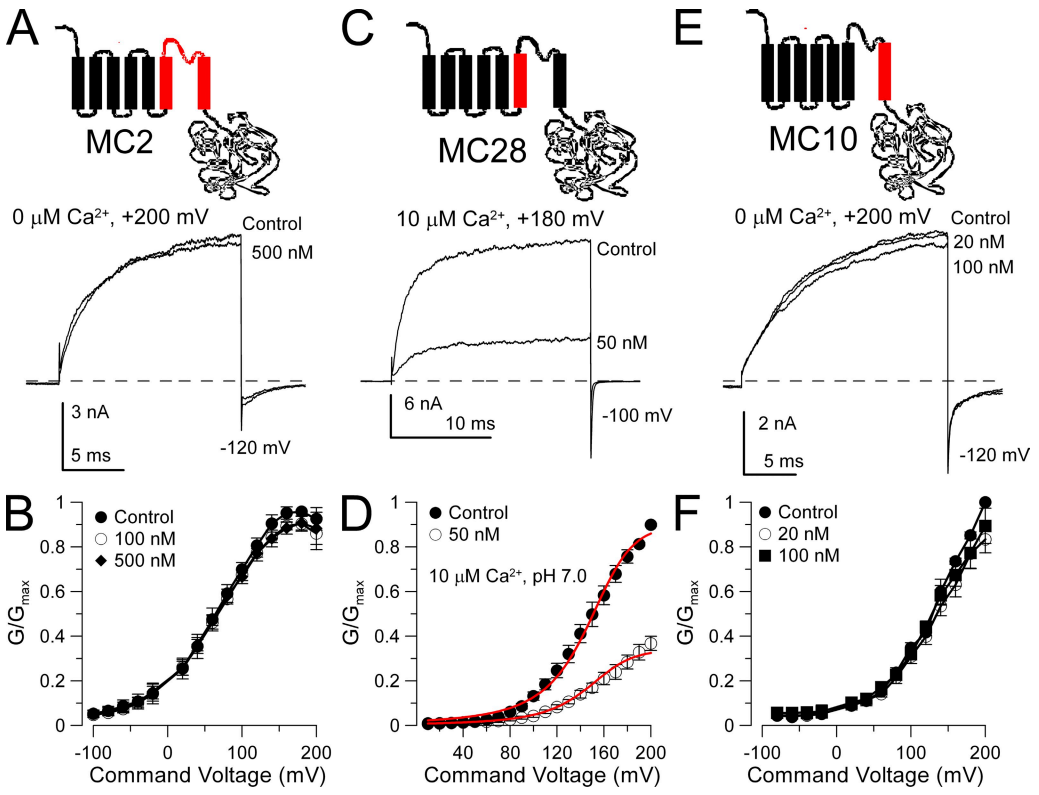

Figure 3. Replacement of the Slo1 S6 segment with the Slo3 sequence abolishes sensitivity to paxilline. (A) Replacing the Slo1 S5–P loop–S6 segment with the homologous Slo3 sequence (chimera MC2) abolishes paxilline sensitivity. The MC2 construct is diagrammed at the top. Traces show MC2 currents activated with 10 μM Ca^{2+} at +200 mV with and without 500 nM paxilline. (B) Paxilline has no effect on MC2 G-V curves ($n = 4$ patches). (C) Paxilline sensitivity persists after replacement of the Slo1 S5 segment with the homologous Slo3 sequence. The MC28 construct is diagrammed at the top. Traces show MC28 currents activated with 10 μM Ca^{2+} at +180 mV with and without paxilline. (D) G-V curves for MC28 with and without 50 nM paxilline ($n = 3$ patches) are shown. Red lines correspond to a fit of Eq. 1, with $K_{bc} = K_{bo} = 30.4 \pm 1.7$ nM with no voltage dependence. (E) Paxilline sensitivity is lost when the Slo1 S6 segment is replaced with the homologous Slo3 sequence. The MC10 construct is diagrammed at the top. Traces show MC10 currents activated with 0 Ca^{2+} at +200 mV with and without paxilline. MC10 is strongly activated by Ca^{2+}, but like Slo3 and MC13, it is also strongly blocked by μM Ca^{2+}. (F) G-V curves are shown for MC10 with and without paxilline ($n = 4$ patches).

Published April 26, 2010

fit with Eq. 1 based on the single concentration of paxilline tested in each case, the block affinities were 6.3 ± 0.3 nM for Slo1 and 4.1 ± 0.1 for MC8. We have noted a similar discrepancy between the rate-based and equilibrium estimates of paxilline block of Slo1 in another set of seven patches, whereas any discrepancy is small for MC8. Although we have no definitive explanation why the rate-based estimate of paxilline block affinity of Slo1 is much weaker than that estimated from the fit of the G-V curves, such a discrepancy might arise if the strict assumption of a first-order blocking reaction was invalid. For present purposes, the differences between paxilline block of Slo1 and MC8 simply serve to point out that the Slo1 pore loop segment impacts on the properties of paxilline block.

A critical residue in Slo1 S6 is necessary and sufficient to permit block by paxilline

Slo1 and Slo3 differ in 10 residues along the portion of the S6 segment that is likely to contribute to the BK central cavity and perhaps the entrance to the cavity (Fig. 6 A). We created two sets of mutations. First, we mutated specific residues in Slo1 S6 to their corresponding Slo3 residue to see whether paxilline sensitivity might be abolished. Second, using the MC10 construct in which a Slo3 S6 replaced the Slo1 S6 segment, we mutated selected non-conserved Slo3 residues to their Slo1 counterpart.

Slo1-G311S was found to completely abolish the ability of 500 nM paxilline to block currents (Fig. 6 B). Similarly, Slo1-G311A was also completely insensitive to paxilline (Fig. 6 C). In contrast, Slo1-A313I (Fig. 6 D) and Slo1-M314L (Fig. 6 E) exhibited sensitivity to paxilline that was similar to native Slo1.

We next attempted to restore paxilline sensitivity to the MC10 construct. When residue S300 in MC10 was mutated to glycine (MC10-S300G), 50 nM paxilline produced strong block (Fig. 7 A) with an estimated K_b = 13.1 ± 0.6 nM (Fig. 7 B), similar to block of wild-type Slo1. When S300G was substituted into MC13, paxilline sensitivity was also restored (Fig. 7 C), but it was less than

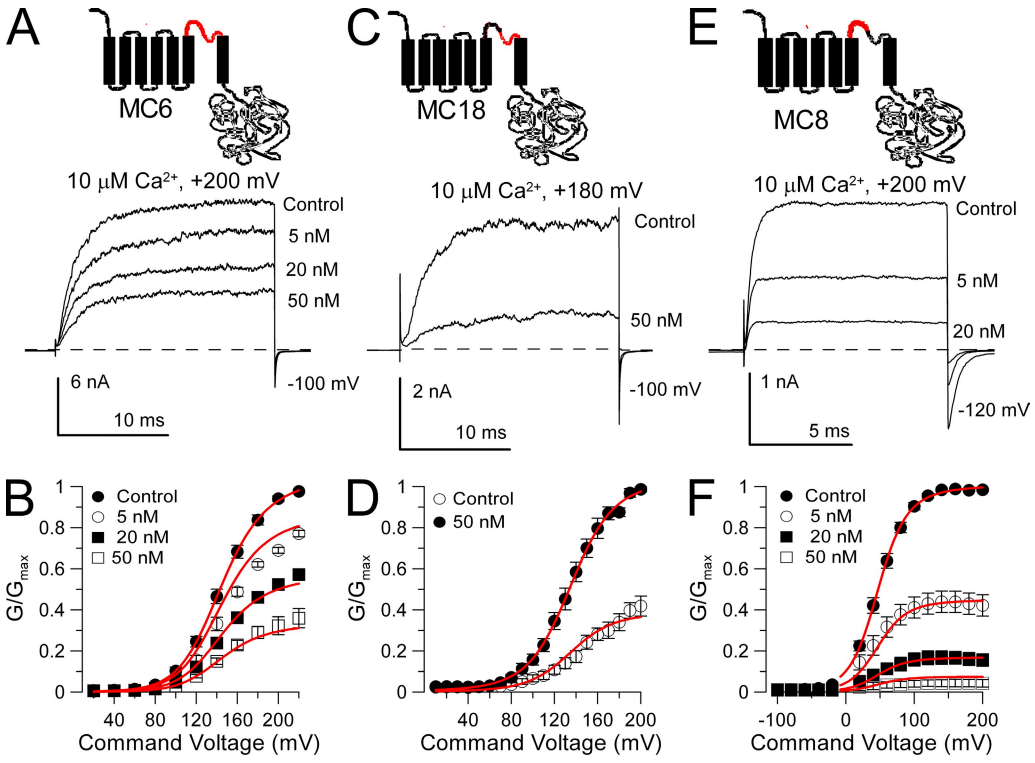

Figure 4. The P loop segment modestly influences paxilline sensitivity. (A) Exchanging the Slo1 P loop with the homologous Slo3 sequence (MC6) on paxilline sensitivity has little or weak effects on paxilline sensitivity. The MC6 construct is schematized on the top. Traces show the effect of various paxilline concentrations on MC6 currents evoked by a step to +200 mV with 10 μM Ca^{2+}. (B) G-V curves are plotted for MC6 with and without paxilline (n = 4–5 patches). The red lines correspond to the best fit of a model in which paxilline blocks both open and closed channels identically (K_b = 23.2 ± 1.0 nM) with no voltage dependence. (C) Replacing the second half of the Slo1 P loop with the homologous Slo3 sequence (MC18) has little effect paxilline sensitivity. The MC18 construct is diagrammed at the top. Traces show MC18 currents activated with 10 μM Ca^{2+} at +180 mV with and without paxilline. (D) G-V curves are plotted for MC18 with and without paxilline (n = 4 patches), with the red lines showing a fit of Eq. 2 with K_b = 30.0 ± 1.4 and z = 0 *e*. (E) Replacing the first half of the Slo1 P loop with the homologous Slo3 sequence (MC8) increases paxilline sensitivity. The MC8 construct is diagrammed at the top. Traces show MC8 currents activated with 10 μM Ca^{2+} at +200 mV in the presence and absence of paxilline. (F) G-V curves are displayed for MC8 with and without paxilline (n = 5 patches). Red lines correspond to a fit of Eq. 1 with equivalent open- and closed-channel block (K_b = 4.04 ± 0.10 nM) with no voltage dependence.

Published April 26, 2010

that observed in wild-type Slo1, with K_b = 170.2 ± 7.2 nM (Fig. 7 D). In contrast, constructs MC10-M311I/V312I, MC10-N306S/I308V, and MC10-T297I were not blocked by 50 nM paxilline. These results again support the idea that the G311(Slo1)/S300(Slo3) position is the key determinant that defines paxilline sensitivity of a construct. Furthermore, the differential ability of the S300G substitution to restore paxilline sensitivity in MC10 and MC13 provides further support for the idea that the pore loop can influence the paxilline block affinity.

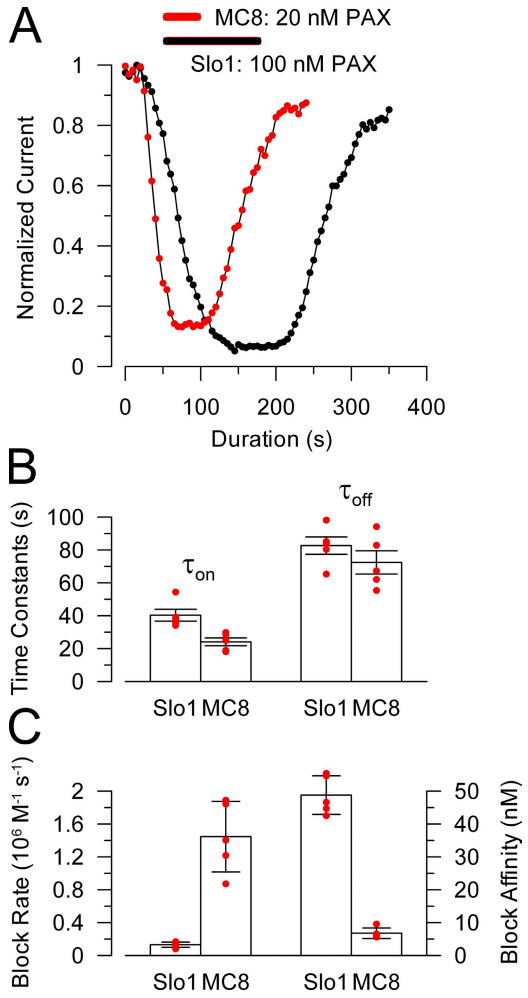

Figure 5. Replacing the first half of the Slo1 P loop with the Slo3 sequence increases paxilline block affinity and speeds up paxilline block and unblock rates. (A) The time course of onset and recovery of paxilline block for Slo1 (black) and MC8 (red) is shown for representative inside-out patches for each construct. For MC8, 20 nM paxillline was applied (horizontal bar), and 100 nM was used for Slo1. Peak current activated at +200 mV was measured every 2 (Slo1) or 3 (MC8) seconds and plotted against time. (B) Time constants of onset of paxilline block (τ_{on}) and recovery (τ_{off}) are plotted for Slo1 (at 100 nM) and MC8 (at 20 nM). Red dots are individual determinations, and bars indicate means and SEM. (C) The forward block rate and paxilline block affinity were calculated for each individual patch for Slo1 and MC8. Block rate (left axis) and affinity (right axis) were determined from $\tau_{on} = 1/([PAX]k_f+k_u)$, $k_u = 1/\tau_{off}$, and $K_b = k_u/k_f$.

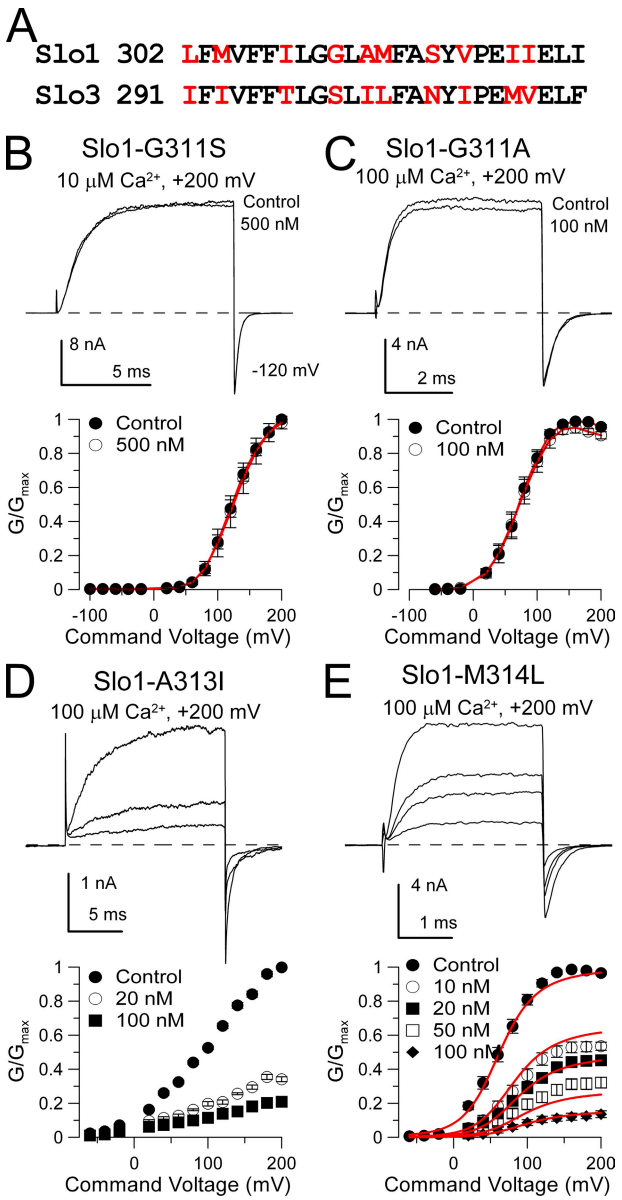

Figure 6. Mutation of glycine 311 in Slo1 S6 abolishes high affinity block by paxilline. (A) A consensus alignment of Slo1 and Slo3 S6 segments is shown. Non-conserved residues are in red. (B) Paxilline is without effect on Slo1-G311S. Currents were activated with 10 μM Ca^{2+} at +200 mV, and 500 nM paxilline produces no effect. On the bottom, G-V curves for Slo1-G311S with and without 500 nM paxilline (n = 3 patches) are plotted. (C) Paxilline is without effects on Slo1-G311A. Currents were activated with 10 μM Ca^{2+} at +200 mV, and 500 nM paxilline had only a minor effect. G-V curves plotted on the bottom also show lack of paxilline effect (n = 5 patches). (D) Paxilline sensitivity persists in Slo1-A313I. Currents activated with 100 μM Ca^{2+} are blocked by 20 and 100 nM paxilline, as also shown in the G-V curves on the bottom (n = 5 patches). (E) Paxilline blocks Slo1-M314L. Currents activated with 100 μM Ca^{2+} are blocked in a concentration-dependent fashion by paxilline, as summarized in the G-V curves on the bottom (n = 8 patches). Red line corresponds to fit with equivalent voltage-independent block of open and closed states with K_b = 13.3 ± 0.80 nM.

Published April 26, 2010

Tests of other factors that might influence paxilline block

Residue G311 is adjacent to a second glycine residue, G310, which is conserved with Slo3 and most other voltage-dependent K^+ channels. To test whether G310 might act similarly in paxilline block, we created a Slo1-G310C construct. Paxilline effectively blocked Slo1-G310C (Fig. 8, A and B), although with a somewhat weaker blocking constant of 34.6 ± 1.8 nM than for wild-type alone. This supports the idea that G311 plays a unique role in permitting paxilline block of Slo1.

We showed above that, although S300G restored paxilline sensitivity to MC13, MC13-S300G was much less sensitive to paxilline than MC10-S300G. Because MC13 was studied with a cytosolic pH of 8.5, whereas MC10-S300G was examined with a cytosolic pH of 7.0, we wished to determine whether pH might also influence block by paxilline. We used a construct termed DN5 (also termed 1P3C in previous work; Xia et al., 2004), in which the complete Slo1 cytosolic domain is replaced by Slo3 sequence. Activation of DN5 currents is enhanced by increases in cytosolic pH, and this construct does not respond to changes in cytosolic Ca^{2+}. We therefore examined the ability of paxilline to block DN5 currents during activation with pH 8.5 at various activation voltages (Fig. 8, C and D). DN5 was strongly blocked by paxilline with an effective K_b = 6.3 ± 0.3 nM. This suggests that the ability of paxilline to block the Slo1 pore domain is neither sensitive to cytosolic pH nor to the nature of the cytosolic domain that is connected to the pore domain. We also compared block by 20 nM paxilline of MC10-S300G with either a cytosolic pH of 7.0

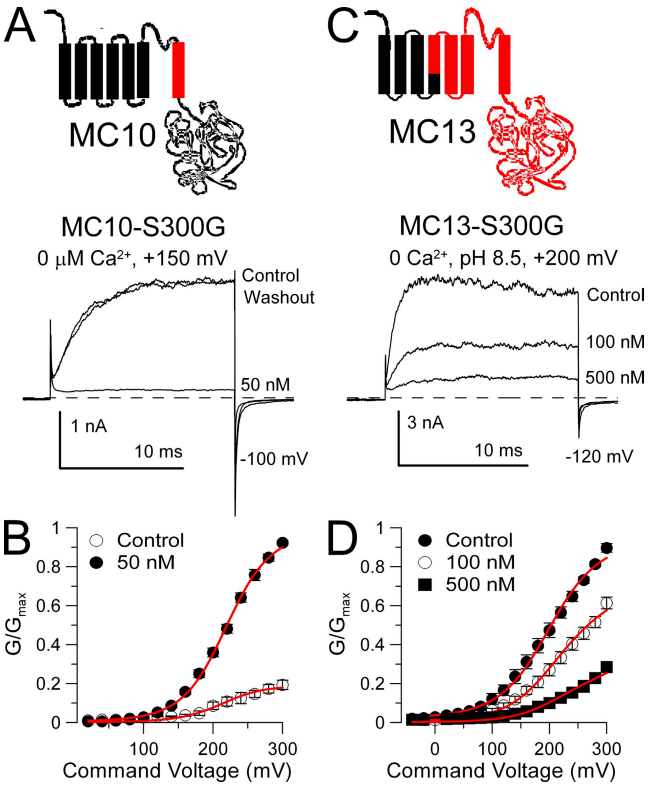

Figure 7. Paxilline sensitivity is restored in constructs with a Slo3 S6 by a glycine at position S300. (A) Paxilline blocks MC10-S300G. 50 nM paxilline markedly inhibits MC10-S300G currents activated at +150 mV with 0 Ca^{2+}. (B) G-V curves are plotted for MC10-S300G with and without 50 nM paxilline (n = 4 patches). Red lines are a fit of Eq. 2 with K_b = 13.1 ± 0.6 nM and no voltage dependence. (C) Paxilline more weakly blocks MC13-S300G. Traces show MC13-S300G currents activated at pH 8.5 at +200 mV. Inhibition occurs with high concentrations of paxilline. (D) G-V curves are plotted for MC13-S300G with and without paxilline (n = 3 patches). Red lines are a fit of Eq. 2 with K_b = 170.2 ± 7.2 nM and no voltage dependence.

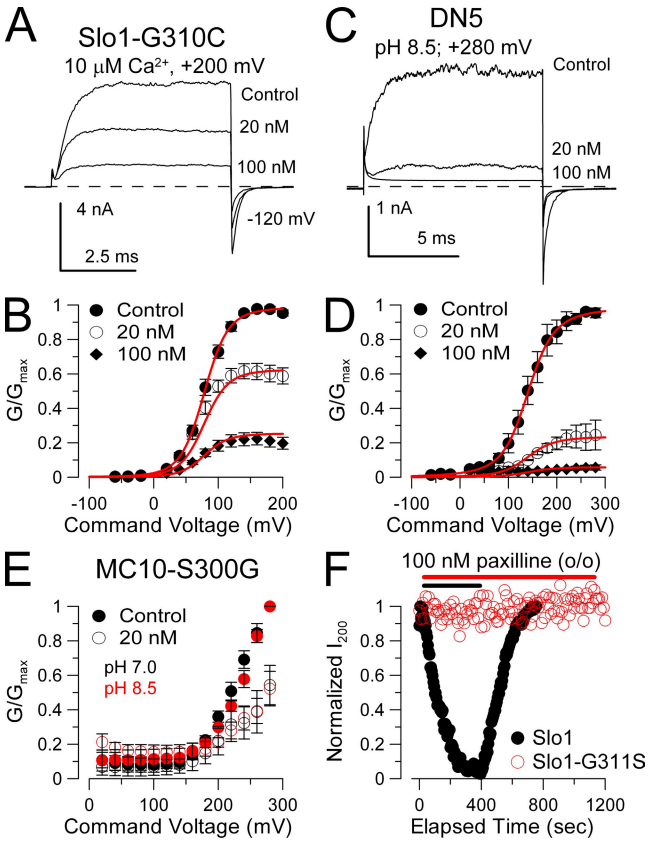

Figure 8. Other tests of factors influencing paxilline block. (A) Paxilline blocks construct Slo1-G310C. Traces show reduction of Slo1-G310C currents by the indicated paxilline concentrations with 10 μM of cytosolic Ca^{2+} and steps to +200 mV. (B) G-V curves are shown for paxilline block of Slo1-G310C. Red line corresponds to fit of voltage-independent block of open and closed states with K_b = 34.6 ± 1.8 nM. (C) Paxilline blocks DN5. Traces show paxilline block of DN5 in which the Slo1 cytosolic structure is replaced by Slo3. Currents were activated with cytosolic pH 8.5 with steps to +280 mV. (D) G-V curves are shown for paxilline block of DN5. Red lines show a fit with K_b = 6.3 ± 0.3 nM with z = 0 e. (E) Paxilline block on MC10-S300G G-V curves is similar at either pH 7.0 (black) or pH 8.5 (red). In both cases, 20 nM paxilline produces similar block. (F) Points plot the peak current during the application of 100 nM paxilline applied to outside-out patches expressing either Slo1 (black) or Slo1-G311S (red). Currents were activated by steps to +200 mV with 10 μM of pipette Ca^{2+} with a holding potential of 0 mV.

Published April 26, 2010

or 8.5 (Fig. 8 E). Block by paxilline was indistinguishable in each case.

Finally, because paxilline is often applied extracellularly to multicellular preparations, we examined the ability of paxilline to block either Slo1 or Slo1-G311S when applied to outside-out patches (Fig. 8 F). In this case, 100 nM paxilline completely blocked Slo1 current, although with a slower onset of block compared with application to inside-out patches. In contrast, 100 nM paxilline was without effect on Slo1-G311S, even after nearly 20 min of application. Thus, regardless of the side of paxilline application, it is sensitive to mutation of G311.

Mutation of G311 also abolishes the BK blocking action of other fungal alkaloids

We also examined whether the ability of three other fungal alkaloids, aflatrem, penitrem A, and verruculogen, to block BK channels (Knaus et al., 1994) was also sensitive to the G311S mutation. 10 nM aflatrem completely blocked BK current (Fig. 9, A and B), while having no effect on Slo1-G311S (Fig. 9, C and D). The blocking effects of penitrem A (Fig. 9, E–H) and verruculogen (Fig. 9, I–L) were also completely ablated by the G311S mutation. Thus, despite the differences in dimensions of each of these alkaloids, these blocking effects are all sensitive to the change in S6 produced by G311 mutation. 10 nM of either aflatrem, penitrem A, or verruculogen blocked BK channels more effectively than 10 nM paxilline. However, at 10 nM, the onset of block of each compound was similar, whereas washout times for aflatrem, penitrem A, and verruculogen were markedly slower than for paxilline.

DISCUSSION

Based on a pronounced difference in paxilline sensitivity between Slo1 and Slo3, we have used a chimeric approach that defined the Slo1 S6 segment as the key element required for blockade by paxilline. Subsequent

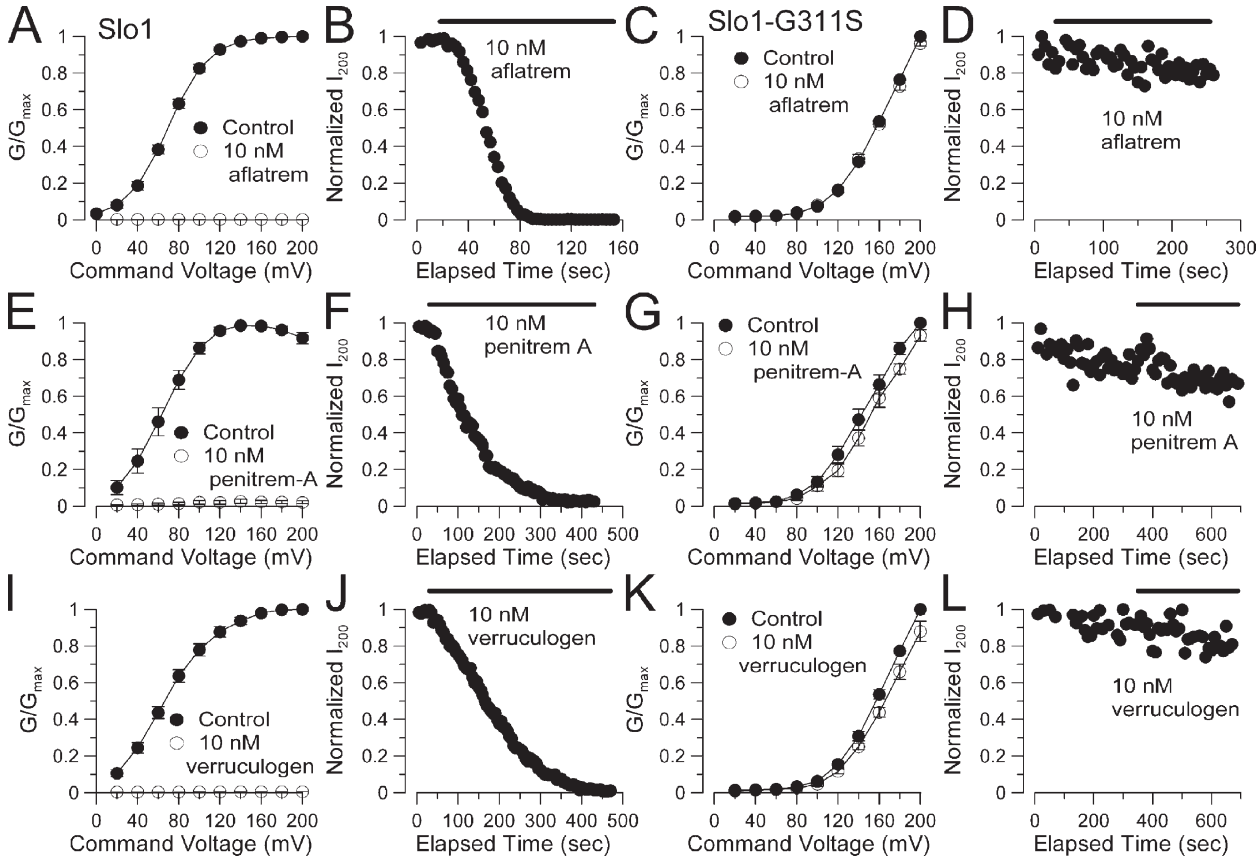

Figure 9. Block of BK channels by other fungal alkaloids is also abolished by the G311S mutation. (A) A Slo1 G-V curve for activation with 10 μM Ca^{2+} is plotted for currents measured in the absence and presence of 10 nM aflatrem ($n = 4$ patches). (B) The time course of block by 10 nM aflatrem is shown for one patch. (C) 10 nM aflatrem is without effect on the G-V elicited by 10 μM Ca^{2+} for the Slo1-G311S construct. (D) Over 4 min of application of 10 nM aflatrem produces no reduction in current of Slo1-G311S. (E) The effect of 10 nM penitrem A on the Slo1 G-V curve is plotted. (F) The time course of block of Slo1 by penitrem A is plotted. (G) 10 nM penitrem A is without effect on Slo1-G311S conductance. (H) Over 5 min of application of 10 nM penitrem A has no effect on Slo1-G311S current. (I) Block of the Slo1 G-V by 10 nM verruculogen is plotted. (J) The time course of verruculogen block is displayed. (K) 10 nM verruculogen is without effect on Slo1-G311S conductance. (L) Over 5 min of verruculogen application is without effect on Slo1-G311S current.

Published April 26, 2010

examination of residues not conserved between Slo1 and Slo3 revealed that mutation of a single glycine residue, G311, in Slo1 S6 completely abolishes paxilline block. Furthermore, replacement in Slo3 S6 of the homologous S300 with glycine at least partially restores paxilline block. In contrast, other S6 residues not conserved between Slo1 and Slo3 had small effects or no substantial effect on paxilline sensitivity. The ability of mutation of a single glycine residue to abolish paxilline sensitivity is quite remarkable, particularly because glycine is unlikely to participate directly in any binding interactions with paxilline. The effect of the G311 mutation seems to point to an important structural difference between the S6 topology in Slo1 and Slo3 that may underlie the differential paxilline sensitivity.

Estimates of paxilline block affinity for various constructs, grouped into order of affinity, are summarized in Table I. We note that Slo1 shares a similar apparent affinity to DN5, Slo1-M314L, and MC10-S300G. That the stronger block affinity for MC8 reflects a real difference is given independent support by the changes in paxilline block rates on MC8 relative to Slo1. Constructs MC6, MC18, MC28, and Slo1-G310C all exhibit somewhat similar paxilline block affinities. However, because these estimates overlap to some extent with estimates for paxilline block of Slo1 that we have observed in some sets of patches (see Materials and methods), their paxilline sensitivity cannot be considered conclusively different from Slo1. Our results do not provide a molecular explanation for the paxilline block mechanism and do not allow firm conclusions regarding the site of paxilline action. Here, we discuss two issues: first, possible implications of the ability of the single glycine residue to influence paxilline block and, second, implications of these results concerning possible sites of paxilline action.

The critical role of G311

The chemical nature of glycine tends to preclude its involvement in any direct interactions with paxilline. A more likely explanation is that mutation of G311 alters the shape or flexibility of the Slo1 S6 in such a way that prevents paxilline from occupying a site that either directly or indirectly produces current block. Glycine is well-known to allow bending or confer flexibility in an otherwise α-helical segment, and the BK channel is unusual in having a pair of sequential glycines at positions 310 and 311. This most certainly would allow for breaking of the hydrogen bonding that maintains an α-helical structure. Interestingly, however, we found that the G310C and G310S mutations produce either small or no effect on paxilline block, indicating that the role of G311 is somehow unique in defining the S6 topology that is critical for paxilline block. A change in S6 topology with mutation of G311 might alter block either by producing a steric hindrance that prevents paxilline from reaching its blocking position, or by resulting in changes in distance between multiple paxilline interaction points. Recent work suggests that the BK channel central cavity may be unusual among voltage-dependent K^+ channels in having a much wider central cavity (Brelidze and Magleby, 2005), and that this central cavity may be

TABLE I

Summary of S5–pore loop–S6 chimeric constructs.

Construct	S5.....turret–pore helix–filter.....S6	K_b
		nM
Slo1		10.6 ± 0.5
MC8		4.04 ± 0.1
DN5		6.3 ± 0.3
Slo1 M314L		13.3 ± 0.8
MC10-S300G		13.1 ± 0.6
MC6		23.2 ± 1.0
MC18		30.0 ± 1.4
MC28		30.4 ± 1.7
Slo1 G310C		34.6 ± 1.8
MC13-S300G		170.2 ± 7.2
MC10		>>100
Slo1-G311S		>>500
MC2		>>500
MC13		>>500

Published April 26, 2010

accessed even when the channel is in closed conformations (Wilkens and Aldrich, 2006; Tang et al., 2009). We imagine that the dimension of the central cavity, at least at some positions along the channel axis, may be related to the pair of sequential glycines found in BK channels.

It is also interesting that the glycine at position 311 in BK channels is shared with a large number of other voltage-gated K^+ channels, both eukaryotic and prokaryotic (Magidovich and Yifrach, 2004). Based on the ability of mutations at this position to alter the closed–open gating equilibrium, this glycine has been termed a gating hinge (Yifrach and MacKinnon, 2002; Magidovich and Yifrach, 2004) that influences the energetics of conformational movements of S6 during the closed-to-open conformational change. Furthermore, it is at the level of the glycine hinge that the S6 helix in the structure of the open MthK channel exhibits a bend (Jiang et al., 2002a,b). Interestingly, Slo3 is one of few K^+ channels that does not have a glycine at this precise position, although it does have a glycine at Slo3 position 299, in alignment with Slo1-G310. Although in some K^+ channels mutation of the hinge glycine results in loss of currents, in BK channels, the G310A and G311A mutations each result in an ∼60-mV positive shift in G-V curves at a given Ca^{2+}, whereas the double mutation shifts gating ∼120 mV (Yifrach and MacKinnon, 2002). Although these considerations do not impact directly on the interpretation of the effects of paxilline, they do suggest that G311 may play a role in conformational changes occurring in S6 during BK gating, perhaps contributing to some unique bend or twist in the BK S6 that distinguishes it from other K^+ channels.

Given that the MC10-S300G and MC13-S300G constructs both exhibit at least some paxilline sensitivity, and assuming that glycine itself is not participating in paxilline binding, we draw two tentative conclusions regarding the ability of the G311/S300 position to influence paxilline block. First, we would suggest that the residues required for paxilline binding are generally shared or conserved between Slo1 and Slo3. Second, the absence of a glycine at the hinge position results in a structural change in S6 that either sterically prevents paxilline from reaching a position that stabilizes its binding or alters the geometric relationship of paxilline contact points, thereby preventing block.

Where is the paxilline blocking position?

Despite the importance of S6 and G311 in paxilline block, we observed that other factors also contribute to paxilline block. First, the presence of the Slo3 sequence in the first half of the pore loop in an otherwise Slo1 subunit influenced paxilline block rates (MC8). This suggests that structural differences or residue differences in the turret region of a BK channel somehow affect the ability of paxilline to reach and leave its binding site. Second, the S300G mutation in MC10 and MC13 did not have identical effects on restoring paxilline sensitivity, suggesting that pore loop differences between MC10 and MC13 alter the ability of paxilline to block. These results may relate to earlier studies in which paxilline block was observed to allosterically influence the binding of scorpion toxins to BK channels (Knaus et al., 1994). Interestingly, different tremorogenic alkaloids were able to either up- or down-regulate CTX binding. Because the turret segment of the BK channel is intimately involved in iberiotoxin binding (Giangiacomo et al., 2008), these earlier results are consistent with our data in supporting the idea that paxilline binding both influences the turret structure and, in turn, the turret structure influences paxilline block. Fig. 2 A highlights those residues in the extracellular part of the BK pore that are thought to influence iberiotoxin binding.

The ability of an S6 mutation to influence paxilline block might be interpreted to suggest that paxilline binds within the central cavity or gains access to its blocking position by entry through the central cavity. Although the large size of paxilline (Fig. 2 A) would seem to argue against the idea that the lipophilic paxilline molecule is able to intercalate into a position between helices, this possibility cannot be totally excluded at present. G311 may be essential for exposing the pathway to reach the appropriate blocking position. In such a case, intercalation might be imagined to influence the pore helix, thereby modifying block by extracellular scorpion toxin. One aspect of paxilline block that does seem unusual in comparison to other standard cytosolic pore blockers is the slow onset and recovery from paxilline block. Block by simple occlusion within the central cavity is presumably mediated by direct exchange with the cytosolic aqueous milieu and, even for an uncharged blocking molecule, that block should occur in accordance with simple diffusion. Our comparison of the blocking kinetics of paxilline on Slo1 and MC8 indicates that, assuming a first-order blocking process, the paxilline block rate of Slo1 is $\sim 0.15 \times 10^6\ M^{-1}\ s^{-1}$, whereas for MC8 we calculated a rate of $\sim 1.4 \times 10^6\ M^{-1}s^{-1}$. This difference in paxilline block rates is unlikely to arise from differences in state occupancy at the holding potential because the V_h for activation of conductance with 10 µM Ca^{2+} is essentially identical for Slo1 and MC8. Although the rate of block of MC8 begins to approximate that seen for diffusionally controlled reactions for larger molecules, the rate of paxilline block for Slo1 seems slower than one would expect for a simple pore occupancy model. Furthermore, that this rate is altered by swapping the Slo1 turret segment with Slo3 turret sequence seems surprising, particularly because the underlying gating equilibria for Slo1 and MC8 are so similar. Although these considerations cannot be considered to rigorously exclude a simple central cavity occupancy basis for paxilline block, both the slow rate of

Published April 26, 2010

block and the ability of the turret segment to influence this rate would be highly unusual features of a strictly simple central cavity occupancy mechanism.

Agricultural problems arising from fungal tremorogenic alkaloids

The compounds examined here are part of a family of fungal alkaloids endemic to range grasses that cause motor disturbances in livestock after ingestion (Miles et al., 1998; Mayland et al., 2007), and block of BK channels has been implicated as the molecular target underlying the tremorogenic effects of these alkaloids (Dalziel et al., 2005; Imlach et al., 2008). We note that the ability of a single point mutation to abolish block of several of these alkaloids raises the possibility that alkaloid sensitivity of livestock could be genetically ablated. Because mutation of G311 is also associated with shifts in G-V curves, this strategy would also require a compensatory mutation, presumably in S6, that produces a normally functioning but toxin-resistant subunit. If such a subunit could be designed, it would result in a physiologically normal animal, resistant to the motor disturbances of the alkaloids.

Summary

We have established that a single amino acid in Slo1 S6, G311, is the key determinant of the ability of paxilline to block BK channels. G311 appears likely to alter structural features of the Slo1 S6 helix that are permissive for paxilline block.

This work was supported by National Institutes of Health grant GM066215 to C.J. Lingle.

Christopher Miller served as editor.

Submitted: 19 January 2010
Accepted: 14 April 2010

REFERENCES

Brelidze, T.I., and K.L. Magleby. 2005. Probing the geometry of the inner vestibule of BK channels with sugars. *J. Gen. Physiol.* 126:105–121. doi:10.1085/jgp.200509286

Cole, R., and R. Cox. 1981. Handbook of Toxic Fungal Metabolites. Academic Press, New York. 937 pp.

Dalziel, J.E., S.C. Finch, and J. Dunlop. 2005. The fungal neurotoxin lolitrem B inhibits the function of human large conductance calcium-activated potassium channels. *Toxicol. Lett.* 155:421–426. doi:10.1016/j.toxlet.2004.11.011

Essin, K., M. Gollasch, S. Rolle, P. Weissgerber, M. Sausbier, E. Bohn, I.B. Autenrieth, P. Ruth, F.C. Luft, W.M. Nauseef, and R. Kettritz. 2009. BK channels in innate immune functions of neutrophils and macrophages. *Blood.* 113:1326–1331. doi:10.1182/blood-2008-07-166660

Giangiacomo, K.M., M.L. Garcia, and O.B. McManus. 1992. Mechanism of iberiotoxin block of the large-conductance calcium-activated potassium channel from bovine aortic smooth muscle. *Biochemistry.* 31:6719–6727. doi:10.1021/bi00144a011

Giangiacomo, K.M., E.E. Sugg, M. Garcia-Calvo, R.J. Leonard, O.B. McManus, G.J. Kaczorowski, and M.L. Garcia. 1993. Synthetic charybdotoxin-iberiotoxin chimeric peptides define toxin binding sites on calcium-activated and voltage-dependent potassium channels. *Biochemistry.* 32:2363–2370. doi:10.1021/bi00060a030

Giangiacomo, K.M., J. Becker, C. Garsky, W. Schmalhofer, M.L. Garcia, and T.J. Mullmann. 2008. Novel alpha-KTx sites in the BK channel and comparative sequence analysis reveal distinguishing features of the BK and KV channel outer pore. *Cell Biochem. Biophys.* 52:47–58. doi:10.1007/s12013-008-9026-3

Horrigan, F.T., and R.W. Aldrich. 2002. Coupling between voltage sensor activation, Ca^{2+} binding and channel opening in large conductance (BK) potassium channels. *J. Gen. Physiol.* 120:267–305. doi:10.1085/jgp.20028605

Imlach, W.L., S.C. Finch, J. Dunlop, A.L. Meredith, R.W. Aldrich, and J.E. Dalziel. 2008. The molecular mechanism of "ryegrass staggers," a neurological disorder of K^+ channels. *J. Pharmacol. Exp. Ther.* 327:657–664. doi:10.1124/jpet.108.143933

Imlach, W.L., S.C. Finch, J. Dunlop, and J.E. Dalziel. 2009. Structural determinants of lolitrems for inhibition of BK large conductance Ca^{2+}-activated K^+ channels. *Eur. J. Pharmacol.* 605:36–45. doi:10.1016/j.ejphar.2008.12.031

Jiang, Y., A. Lee, J. Chen, M. Cadene, B.T. Chait, and R. MacKinnon. 2002a. Crystal structure and mechanism of a calcium-gated potassium channel. *Nature.* 417:515–522. doi:10.1038/417515a

Jiang, Y., A. Lee, J. Chen, M. Cadene, B.T. Chait, and R. MacKinnon. 2002b. The open pore conformation of potassium channels. *Nature.* 417:523–526. doi:10.1038/417523a

Knaus, H.G., O.B. McManus, S.H. Lee, W.A. Schmalhofer, M. Garcia-Calvo, L.M. Helms, M. Sanchez, K. Giangiacomo, J.P. Reuben, A.B. Smith III, et al. 1994. Tremorgenic indole alkaloids potently inhibit smooth muscle high-conductance calcium-activated potassium channels. *Biochemistry.* 33:5819–5828. doi:10.1021/bi00185a021

Long, S.B., E.B. Campbell, and R. Mackinnon. 2005. Crystal structure of a mammalian voltage-dependent Shaker family K^+ channel. *Science.* 309:897–903. doi:10.1126/science.1116269

Magidovich, E., and O. Yifrach. 2004. Conserved gating hinge in ligand- and voltage-dependent K+ channels. *Biochemistry.* 43:13242–13247. doi:10.1021/bi048377v

Mayland, H., P. Cheeke, W. Majak, and J. Goff. 2007. Forage-induced animal disorders. *In* Forages: The Science of Grassland Agriculture. R. Barnes, C. Nelson, K. Moore, and M. Collins, editors. Blackwell Publishing, Aimes, IA. 687–707.

Meera, P., M. Wallner, and L. Toro. 2000. A neuronal beta subunit (KCNMB4) makes the large conductance, voltage- and Ca^{2+}-activated K^+ channel resistant to charybdotoxin and iberiotoxin. *Proc. Natl. Acad. Sci. USA.* 97:5562–5567. doi:10.1073/pnas.100118597

Miles, C.O., M.E. di Menna, S.W. Jacobs, I. Garthwaite, G.A. Lane, R.A. Prestidge, S.L. Marshall, H.H. Wilkinson, C.L. Schardl, O.J. Ball, and G.C. Latch. 1998. Endophytic fungi in indigenous Australasian grasses associated with toxicity to livestock. *Appl. Environ. Microbiol.* 64:601–606.

Pettersen, E.F., T.D. Goddard, C.C. Huang, G.S. Couch, D.M. Greenblatt, E.C. Meng, and T.E. Ferrin. 2004. UCSF Chimera—a visualization system for exploratory research and analysis. *J. Comput. Chem.* 25:1605–1612.

Raffaelli, G., C. Saviane, M.H. Mohajerani, P. Pedarzani, and E. Cherubini. 2004. BK potassium channels control transmitter release at CA3-CA3 synapses in the rat hippocampus. *J. Physiol.* 557:147–157. doi:10.1113/jphysiol.2004.062661

Sali, A., and T.L. Blundell. 1993. Comparative protein modelling by satisfaction of spatial restraints. *J. Mol. Biol.* 234:779–815.

Sanchez, M., and O.B. McManus. 1996. Paxilline inhibition of the alpha-subunit of the high-conductance calcium-activated potassium channel. *Neuropharmacology.* 35:963–968. doi:10.1016/0028-3908(96)00137-2

Published April 26, 2010

Schreiber, M., A. Wei, A. Yuan, J. Gaut, M. Saito, and L. Salkoff. 1998. Slo3, a novel pH-sensitive K^+ channel from mammalian spermatocytes. *J. Biol. Chem.* 273:3509–3516. doi:10.1074/jbc.273.6.3509

Shao, L.R., R. Halvorsrud, L. Borg-Graham, and J.F. Storm. 1999. The role of BK-type Ca^{2+}-dependent K^+ channels in spike broadening during repetitive firing in rat hippocampal pyramidal cells. *J. Physiol.* 521:135–146. doi:10.1111/j.1469-7793.1999.00135.x

Tammaro, P., A.L. Smith, S.R. Hutchings, and S.V. Smirnov. 2004. Pharmacological evidence for a key role of voltage-gated K^+ channels in the function of rat aortic smooth muscle cells. *Br. J. Pharmacol.* 143:303–317. doi:10.1038/sj.bjp.0705957

Tang, Q.Y., X.-H. Zeng, and C.J. Lingle. 2009. Closed-channel block of BK potassium channels by bbTBA requires partial activation. *J. Gen. Physiol.* 134:409–436. doi:10.1085/jgp.200910251

Tang, Q.-Y., Z. Zhang, X.-M. Xia, and C.J. Lingle. 2010. Block of mouse Slo1 and Slo3 K^+ channels by CTX, IBX, TEA, 4-AP, and quinidine. *Channels.* 4:22–41.

Wilkens, C.M., and R.W. Aldrich. 2006. State-independent block of BK channels by an intracellular quaternary ammonium. *J. Gen. Physiol.* 128:347–364. doi:10.1085/jgp.200609579

Xia, X.-M., J.P. Ding, and C.J. Lingle. 1999. Molecular basis for the inactivation of Ca^{2+}- and voltage-dependent BK channels in adrenal chromaffin cells and rat insulinoma tumor cells. *J. Neurosci.* 19:5255–5264.

Xia, X.-M., J.-P. Ding, X.-H. Zeng, K.-L. Duan, and C.J. Lingle. 2000. Rectification and rapid activation at low Ca^{2+} of Ca^{2+}-activated, voltage-dependent BK currents: consequences of rapid inactivation by a novel β subunit. *J. Neurosci.* 20:4890–4903.

Xia, X.-M., X. Zhang, and C.J. Lingle. 2004. Ligand-dependent activation of Slo family channels is defined by interchangeable cytosolic domains. *J. Neurosci.* 24:5585–5591. doi:10.1523/JNEUROSCI.1296-04.2004

Yifrach, O., and R. MacKinnon. 2002. Energetics of pore opening in a voltage-gated K(+) channel. *Cell.* 111:231–239. doi:10.1016/S0092-8674(02)01013-9

Zhang, X., C.R. Solaro, and C.J. Lingle. 2001. Allosteric regulation of BK channel gating by Ca^{2+} and Mg^{2+} through a nonselective, low affinity divalent cation site. *J. Gen. Physiol.* 118:607–636. doi:10.1085/jgp.118.5.607

Zhang, X., X.-H. Zeng, and C.J. Lingle. 2006a. Slo3 K^+ channels: voltage and pH dependence of macroscopic currents. *J. Gen. Physiol.* 128:317–336. doi:10.1085/jgp.200609552

Zhang, X., X.-H. Zeng, X.-M. Xia, and C.J. Lingle. 2006b. pH-regulated Slo3 K^+ channels: properties of unitary currents. *J. Gen. Physiol.* 128:301–315. doi:10.1085/jgp.200609551